Int. J. Electrochem. Sci., 8 **(2013)** 11512 - 11525

International Journal of
ELECTROCHEMICAL
SCIENCE
www.electrochemsci.org

Adsorption and Corrosion Inhibition of Steel in Hydrochloric Acid Solution by 3-bromo-2-phenylimidazol[1,2- α] pyridine.

A. Anejjar[1], *R. Salghi*[1,*], *A. Zarrouk*[2], *O. Benali*[3], *H. Zarrok*[4], *B. Hammouti*[2], *S. S. Al-Deyab*[5], *N. Benchat* [2], *A. Elaatiaoui* [2].

[1] Laboratory of Environmental Engineering and Biotechnology, ENSA, Université Ibn Zohr, PO Box 1136, 80000 Agadir, Morocco
[2] LCAE-URAC 18, Faculty of Science, University of Mohammed Premier, Po Box 717 60000 Oujda, Morocco.
[3] Department of Biology, Faculty of Sciences and technology, Saïda University, Algeria
[4]Laboratory separation processes, Faculty of Science, University Ibn Tofail PO Box 242, Kenitra, Morocco.
[5]Petrochemical Research Chair, Chemistry Department, College of Science, King Saud University, P.O. Box 2455, Riyadh 11451, Saudi Arabia.
[*]E-mail: r_salghi@yahoo.fr

Received: 4 March 2013 / *Accepted:* 7 August 2013 / *Published:* 20 August 2013

The inhibition performance of the 3-bromo-2-phenylimidazol[1,2- α] pyridine (BPP) on mild steel in normal hydrochloric acid medium (1 M HCl) at 298 K was tested by weight loss, potentiodynamic polarisation and electrochemical impedance spectroscopy (EIS) techniques. This organic compound inhibits the acidic corrosion even at low concentration, reaching a value of inhibition efficiency up to 86% at a concentration of 10^{-3} M. The results obtained from the different corrosion evaluation techniques are in good agreement. Polarisation curves indicate that BPP is a mixed inhibitor, affecting both cathodic and anodic corrosion currents. Data, obtained from EIS measurements, were analyzed to model the corrosion inhibition process through appropriate equivalent circuit model. The adsorption of BPP on the steel surface, in 1 M HCl solution, obeys to Langmuir's isotherm with a very high negative value of the free energy of adsorption $\Delta G°_{ads}$. The effect of the temperature on the corrosion behavior with addition of 10^{-3} M of the inhibitor was studied in the temperature range 298-328 K. Activation energies in the presence and absence of BPP were obtained by measuring the temperature dependence of the charge transfer resistance.

Keywords: Corrosion, Inhibition, Steel, HCl, EIS

1. INTRODUCTION

Hydrochloric acid solutions are widely used for the pickling, cleaning, descaling and etching of mild steel [1-3]. Steel is widely used in most industries because of its low cost and availability for

the manufacture of reaction vessels such as cooling tower reservoirs, pipelines, etc… [4]. The use of inhibitor is one of the most practical methods to protect metals from corrosion, especially in aggressive media [5-7]. Organic inhibitors containing nitrogen, oxygen and/or sulfur have been widely used for steel, copper and iron [8-22]. These compounds and its derivatives are excellent corrosion inhibitors for steel in acidic media [23-29]. The inhibiting performance of this inhibitor was evaluated by polarization curves, weight loss and EIS. The chemical structure of the studied 3-bromo-2-phenylimidazol[1,2- α]pyridine (**BPP**) derivative is given in Fig 1.

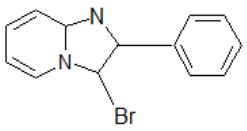

Figure 1. 3-bromo-2-phenylimidazol[1,2- α] pyridine (**BPP**)

2. MATERIALS AND METHODS

2.1. Materials

The steel used in this study is a carbon steel (Euronorm: C35E carbon steel and US specification: SAE 1035) with a chemical composition (in wt%) of 0.370 % C, 0.230 % Si, 0.680 % Mn, 0.016 % S, 0.077 % Cr, 0.011 % Ti, 0.059 % Ni, 0.009 % Co, 0.160 % Cu and the remainder iron (Fe). The carbon steel samples were pre-treated prior to the experiments by grinding with emery paper SiC (120, 600 and 1200); rinsed with distilled water, degreased in acetone in an ultrasonic bath immersion for 5 min, washed again with bidistilled water and then dried at room temperature before use. The acid solutions (1.0 M HCl) were prepared by dilution of an analytical reagent grade 37 % HCl with double-distilled water. The concentration range of 3-bromo-2-phenylimidazol [1,2- α] pyridine employed was 10^{-6} M to 10^{-3} M.

2.2. Measurements

2.2.1. Weight loss measurements

The gravimetric measurements were carried out at definite time interval of 6 h at room temperature using an analytical balance (precision ± 0.1 mg). The carbon steel specimens used have a rectangular form (length = 1.6 cm, width = 1.6 cm, thickness = 0.07 cm). Gravimetric experiments were carried out in a double glass cell equipped with a thermostated cooling condenser containing 80 mL of non-de-aerated test solution. After immersion period, the steel specimens were withdrawn, carefully rinsed with bidistilled water, ultrasonic cleaning in acetone, dried at room temperature and then weighted. Triplicate experiments were performed in each case and the mean value of the weight loss was calculated.

2.2.2. Electrochemical measurements

Electrochemical experiments were conducted using impedance equipment (Tacussel-Radiometer PGZ 100) and controlled with Tacussel corrosion analysis software model Voltamaster 4. A conventional three-electrode cylindrical Pyrex glass cell was used. The temperature is thermostatically controlled. The working electrode was carbon steel with the surface area of 1 cm^2. A saturated calomel electrode (SCE) was used as a reference. All potentials were given with reference to this electrode. The counter electrode was a platinum plate of surface area of 1 cm^2. A saturated calomel electrode (SCE) was used as the reference; a platinum electrode was used as the counter-electrode. All potentials are reported *vs*. SCE. All electrochemical tests have been performed in aerated solutions at 298 K.

For polarization curves, the working electrode was immersed in a test solution during 30 min until a steady state open circuit potential (E_{ocp}) was obtained. The polarization curve was recorded by polarization from -800 to -200 mV/SCE with a scan rate of 1 mV s^{-1}. AC impedance measurements were carried-out in the frequency range of 100 kHz to 10 mHz, with 10 points per decade, at the rest potential, after 30 min of acid immersion, by applying 10 mV ac voltage peak-to-peak. Nyquist plots were made from these experiments. The best semicircle can be fit through the data points in the Nyquist plot using a non-linear least square fit so as to give the intersections with the *x*-axis.

3. RESULTS AND DISCUSSION

3.1. Polarization measurements

Potentiodynamic anodic and cathodic polarization scans were carried out at 289 K in 1 M HCl with different concentrations of **BPP**. Anodic and cathodic polarization curves in the absence and in the presence of inhibitors at different concentrations after 0.5 h of immersion and at 298 K are shown in Figure 2.

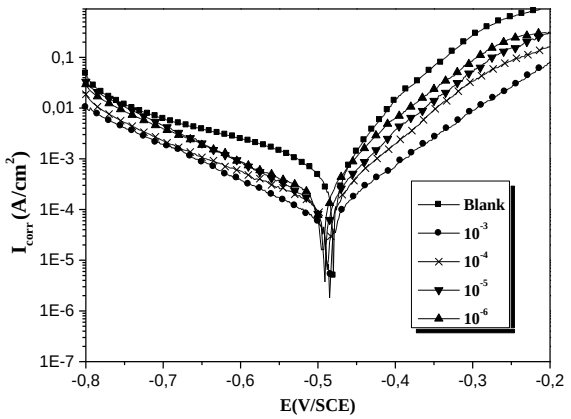

Figure 2. Potentiodynamic polarisation curves of C38 steel in 1M HCl in the presence of different concentrations of **BPP**

Table 1 gives the values of kinetic corrosion parameters as the corrosion potential E_{corr}, corrosion current density I_{corr}, Tafel slope b_c, and inhibition efficiency for the corrosion of C38 steel in 1 M HCl with different concentrations of **BPP**.

Table 1. Electrochemical parameters of C38 steel at various concentrations of **BPP** in 1M HCl and corresponding inhibition efficiency.

Conc. (M)	$-E_{corr}$ (mV/SCE)	I_{corr} ($\mu A/cm^2$)	$-b_c$ (mV/dec)	P (%)
Blank	536	355	150	----
10^{-3}	485	50	187	85.91
10^{-4}	488	108	143	69.58
10^{-5}	491	130	137	63.38
10^{-6}	494	175	164	50.70

The corrosion current densities were estimated by Tafel extrapolation of the cathodic curves to the open circuit corrosion potential. The inhibition efficiency was then calculated using the expression:

$$P\% = \frac{I^0_{corr} - I_{corr}}{I^0_{corr}} x100 \qquad (1)$$

where I^0_{corr} is the corrosion current density in uninhibited acid and I_{corr} is the corrosion current density in inhibited acid.

Table 1 shows that an increase in inhibitor concentration is resulted in increased inhibition efficiency. It is evident from the results that:

- I_{corr} values decrease considerably in the presence of inhibitor. Thus, P (%) increases with inhibitor concentration, reaching the values **85.91** at 10^{-3} M.
- The values of b_c and E_{corr} remained almost unchanged on increasing the concentration of **BPP**.
- In the anodic range (Figure 2), **BPP** influenced the anodic reactions for an overvoltage higher than E_{corr} This result indicated that **BPP** exhibits both cathodic and anodic inhibition effects. This suggested a mixed-type control and **BPP** mainly acts as a mixed-type inhibitor in 1 M HCl, the same phenomenon has been reported by Bentiss et al. with 3,5-diphenyl-4H-1,2,4-triazole in 1 M HCl [30].

3.2. Electrochemical impedance spectroscopy measurements

The corrosion behaviour of C38 steel, in acidic solution in the presence of **BPP**, was investigated by the EIS methods at 298 K. Nyquist plots obtained for frequencies ranging from 100 kHz to 10 mHz at open circuit potential for C38 steel in 1 M HCl in the presence of various concentrations of **BPP** are shown in Figure 3. The impedance diagrams obtained are not perfect

semicircles and the difference was attributed to frequency dispersion [22**]**. The fact that impedance diagrams have a semicircular appearance shows that the corrosion of steel is controlled by a charge transfer process. The equivalent circuit model employed for this system is presented in Figure 4. The resistance R_s is the resistance of the solution; R_t reflects the charge transfer resistance and C_{dl} is the double - layer capacitance.

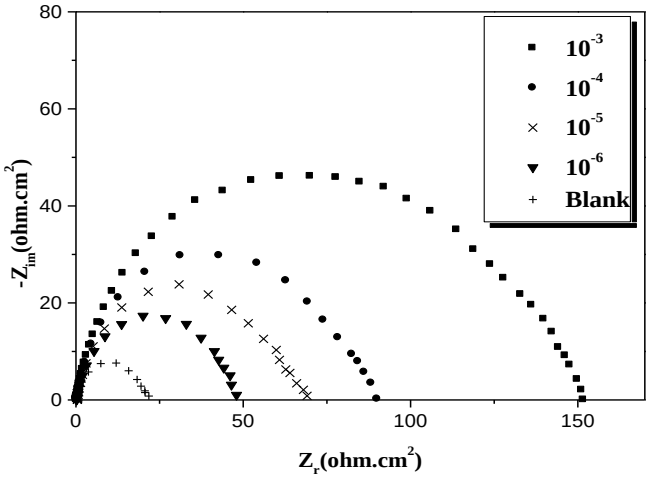

Figure 3. Nyquist diagrams for C38 steel electrode with and without **BPP** at E_{corr} after 30 min of immersion.

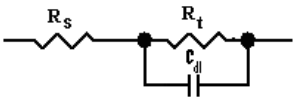

Figure 4. The electrochemical equivalent circuit used to fit the impedance spectra.

Values of the charge transfer resistance R_t were obtained from these plots by determining the difference in the values of impedance at low and high frequencies as suggested by Tsuru and Haruyama [31]. Values of the double–layer capacitance C_{dl} were calculated from the frequency at which the impedance imaginary component $-Z_i$ is maximum using the equation:

$$f(-Zi_{max}) = \frac{1}{2\pi C_{dl} R_t} \qquad (2)$$

The percent inhibition efficiency is calculated by charge transfer resistance obtained from Nyquist plots, according to the equation:

$$P\ \% = \frac{R'_t - R_t}{R'_t} \times 100 \qquad (3)$$

where R_t and R'_t are the charge transfer resistance values without and with inhibitor, respectively.

Table 2 gives the values of the charge transfer resistance R_t, double layer capacitance C_{dl}, and inhibition efficiency obtained from the above plots.

Table 2. Electrochemical Impedance parameters for corrosion of steel in acid medium at various contents of BPP.

Conc. (M)	R_t ($\Omega.cm^2$)	f_{max} (Hz)	C_{dl} ($\mu F/cm^2$)	P (%)
Blank	21	89	85.19	-----
10^{-3}	152	31	33.79	86.18
10^{-4}	90	50	35.39	76.67
10^{-5}	69	50	46.15	69.56
10^{-6}	48	50	66.35	56.25

It can be seen that the presence of **BPP** enhances the values of R_t and reduces the C_{dl} values. The decrease in C_{dl}, which can result from a decrease in local dielectric constant and / or an increase in the thickness of the electric double layer [29], suggested that **BPP** molecules function by adsorption at the metal / solution interface. Thus, the decrease in C_{dl} values and the increase in R_t values and consequently of inhibition efficiency may be due to the gradual replacement of water molecules by the adsorption of the inhibitor molecules on the metal surface, decreasing the extent of dissolution reaction [32-33]. This compound can be adsorbed on the metal surface by the interaction between lone pairs of electrons of nitrogen and brome atoms of the inhibitor and the metal surface or via interaction of **BPP** with already adsorbed chloride ions [20, 34]. This process is facilitated by the presence of vacant orbitals of low energy in iron atom, as observed in the transition group metals [10]. Ashassi-Sorkhabi and Nabavi-Amri [35] proposed the following mechanism involving two adsorbed intermediates to account for the retardation of Fe anodic dissolution in the presence of an inhibitor:

$$Fe + H_2O \rightleftharpoons Fe\,H_2O_{ads} \quad (4a)$$

$$Fe\,H_2O_{ads} + \mathbf{BPP} \rightleftharpoons Fe\,OH^-_{ads} + H^+ + \mathbf{BPP} \quad (4b)$$

$$Fe\,H_2O_{ads} + \mathbf{BPP} \rightleftharpoons Fe\mathbf{BPP}_{ads} + H_2O \quad (4c)$$

$$Fe\,OH^-_{ads} \xrightarrow{rds} Fe\,OH_{ads} + e \quad (4d)$$

$$Fe\,\mathbf{BPP}_{ads} \rightleftharpoons Fe\mathbf{BPP}^+_{ads} + e \quad (4e)$$

$$Fe\,OH_{ads} + Fe\,\mathbf{BPP}^+_{ads} \rightleftharpoons Fe\,\mathbf{BPP}_{ads} + Fe\,OH^+ \quad (4f)$$

$$Fe\,OH^+ + H^+ \rightleftharpoons Fe^{2+} + H_2O \quad (4g)$$

Considering the inhomogeneous nature of metallic surfaces resulting from the existence of lattice defects and dislocations, a corroding metal surface is generally characterized by multiple adsorption sites having activation energies and heats of adsorption. Inhibitor molecules may thus be adsorbed more readily at surface active sites having suitable adsorption enthalpies. According to the detailed mechanism above, displacement of some adsorbed water molecules on the metal surface by inhibitor species to yield the adsorbed intermediate FeM_{ads} (Eq. (6c)) reduces the amount of the species $FeOH^-_{ads}$ available for the rate-determining steps and consequently retards Fe anodic dissolution [36].

3.3 Weight loss, corrosion rates and inhibition efficiency

Values of the inhibition efficiency and corrosion rate obtained from the weight loss measurements of C38 steel for different concentrations of **BPP** in 1 M HCl at 298 K after 6 h of immersion are given in Table 3. The inhibition efficiency is defined as follows:

$$P\ \% = \frac{W_{corr} - W'_{corr}}{W_{corr}} \times 100 \qquad (5)$$

where W_{corr} and W'_{corr} are the corrosion rates of steel due to the dissolution in 1 M HCl in the absence and the presence of definite concentration of inhibitor, respectively.

Table 3. Effect of **BPP** concentration on corrosion data of carbon steel in 1 M HCl.

Conc. (M)	W_{corr} (mg cm^{-2} h^{-1})	P (%)
Blank	1.00	----
10^{-3}	0.14	86.00
10^{-4}	0.26	74.00
10^{-5}	0.35	65.00
10^{-6}	0.38	62.00

It is obvious from the Table 1 that the **BPP** inhibit the corrosion of C38 steel in 1 M HCl solution at all concentrations used in this study and the corrosion rate (W) is seen to decrease continuously with increasing additive concentration at 289K. Indeed, corrosion rate values of C38 steel decrease when the inhibitor concentration increases while P(%) values of **BPP** increase with the increase of the concentration, the maximum P(%) of 86 % is achieved at 10^{-3} M.

3.4. Adsorption isotherm

The inhibitor efficiency depends on the type and number of active sites at metal surface, the charge density, the molecular size of the inhibitor, the metal–inhibitor interaction, and the metallic complex formation. The adsorption isotherm can give information on the metal–inhibitor interaction [28]. The adsorption isotherm can be derived from the curve surface coverage against inhibitor concentration. Surface coverage was estimated as Eq. 5. The θ values for different inhibitor concentrations are tested by fitting to various isotherms. By far the best fit was obtained with the Langmiur isotherm. According to this isotherm θ is related to concentration inhibitor C via :

$$\frac{C}{\theta} = \frac{1}{K} + C \qquad (6)$$

with

$$K = \frac{1}{55,5} \exp\left(-\frac{\Delta G^{0}_{ads}}{RT}\right) \qquad (7)$$

where K is the adsorptive equilibrium constant and $\Delta G°_{ads}$ the free energy of adsorption**.**

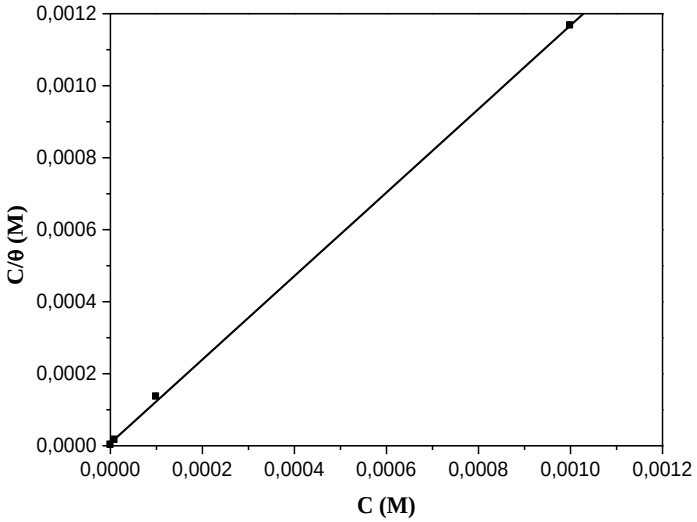

Figure 5. Plots of Langmuir adsorption isotherm of BPP on the steel surface at 298K.

It was found that figure 5 (plot of $\frac{C}{\theta}$ versus C) gives straight line. The obtained results indicate that the adsorption of compound under consideration on C38 steel/acidic solution interface follows the Langmuir adsorption isotherm. The obtained results are given in table 4.

Table 4. The thermodynamic parameters for of carbon steel in 1 M HCl in the absence and presence of different concentrations of **BPP**

Inhibitor	Slope	K_{ads} (M^{-1})	R^2	ΔG°_{ads} (kJ/mol)
BPP	1.1	1.32 x10^5	0.999	-39.14

Inspection of the data of the table 4 shows the following adsorption characteristics of **BPP** in 1 M HCl :

- A value of slope is nearly to the unity indicating that each molecule of the inhibitor is attached to one active site of the steel surface.
- The factor regression is equal to 0.999 which confirms the application of the Langmuir model
- The negative value ΔG_{ads} show that the adsorption of **BPP** is a spontaneous process under the experimental conditions described and also the strong interaction between inhibitor molecules and the metal surface [20, 37-39]. It generally accepted that the values of ΔG_{ads} up to -20 kJ /mol, the types of adsorption were regarded as physisorption, the inhibition acts due to the electrostatic interactions between the charged molecules and the charged metal, while the values around -40 kJ/mol or smaller, were seen as chemisorption, which is due to the charge sharing or a transfer from the inhibitor molecules to the metal surface to form a covalent bond [40-41]. The values of ΔG_{ads} in our

case is 39.14 kJ/mol, it is suggested that the adsorption of this imidazole derivative involves the chemisorption interaction.

3.5. Effect of temperature on corrosion of C38 *steel*

To investigate the mechanism of inhibition and to calculate the activation energies of the corrosion process, EIS measurements were taken at various temperatures in the absence and the presence of the optimal concentration (Figures 6 and 7). Corresponding data are given in table 5.

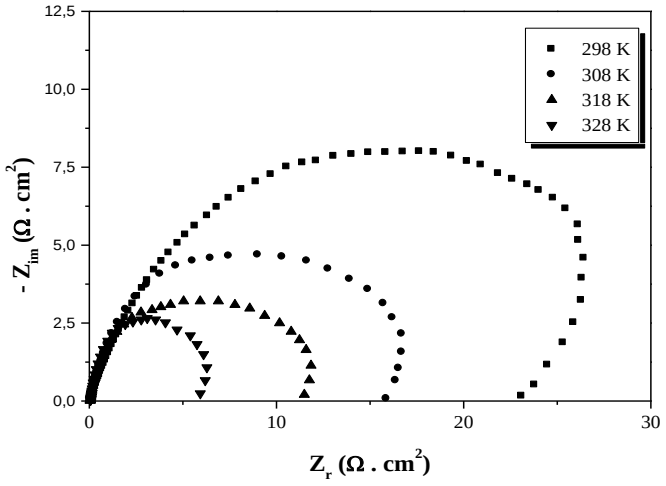

Figure 6. Nyquist diagrams for C38 steel in 1 M HCl at different temperatures.

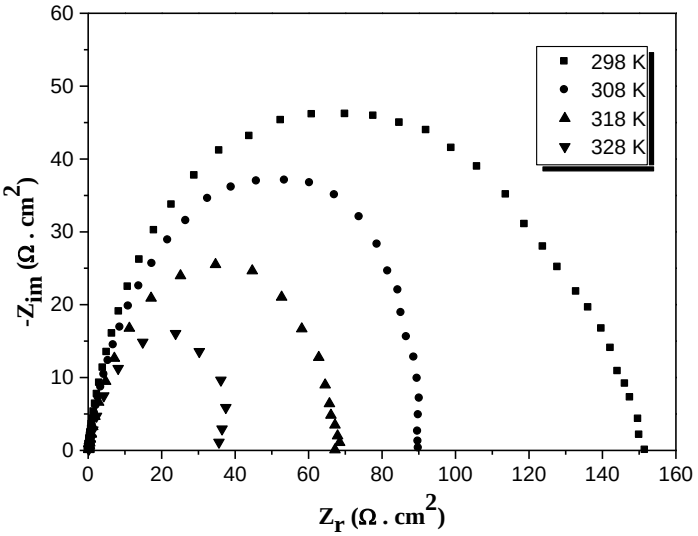

Figure 7. Nyquist diagrams for C38 steel in 1 M HCl + 10^{-3} M of **BPP** at different temperatures.

Corresponding data are given in Table 5. In the studied temperature range (298–328 K) the values of R_t decreases with increasing temperature both in uninhibited and inhibited solutions and the

values of the inhibition efficiency of **BPP** decrease slightly with increasing temperature. The R_t value of C38 steel increases more rapidly with temperature in the presence of the inhibitor, these results confirm that **BPP** acts as an efficient inhibitor in the range of temperature studied.

Table 4. Thermodynamic parameters for the adsorption of BPP at 10^{-3} M in 1 M HCl on the C38 steel at different temperatures.

Inhibitor	Temp (K)	R_{ct} ($\Omega.cm^2$)	f_{max}(Hz)	C_{dl} ($\mu F/cm^2$)	E_{Rct} (%)
Blank	298	21	89	85.19	----
	308	13	152	80.58	----
	318	10	244	65.26	----
	328	5	588	50.15	----
BPP	298	152	31	33.79	86.18
	308	89	25	71.56	85.39
	318	67	30	79.22	85.07
	328	35	50	90.99	84.57

The activation parameters for the corrosion process were calculated from Arrhenius type plot according to the following equation:

$$\ln \frac{1}{R_t} = -\frac{E_a}{RT} + \log A \qquad (8)$$

where E_a is the apparent activation energy, A the pre-exponential factor, R the universal gas constant and T the absolute temperature.

The variations of $\ln 1/R_t$ in 1 M HCl containing various concentrations of **BPP** used with reciprocal of the absolute temperature are presented in figure 8. Straight lines with coefficients of correlation (c. c) higher to 0.98 are obtained.

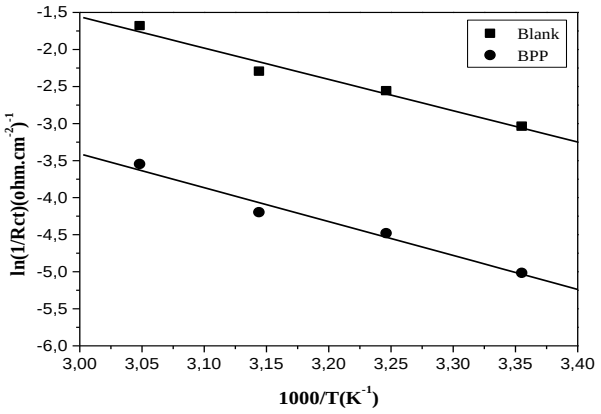

Figure 8. Arrhenius plots of steel in 1 M HCl with and without 10^{-3} mol/l of **BPP**

The adsorption phenomenon has been successfully explained by thermodynamic parameter, to further elucidate the inhibition properties of inhibitor, the kinetic model was another useful tool to explain the mechanism of corrosion inhibition for the inhibitor. The activation parameters for the corrosion process were calculated from Arrhenius equation:

$$1/R_t = \frac{RT}{Nh}\exp\left(\frac{\Delta S_a^*}{R}\right)\exp\left(\frac{\Delta H_a^*}{RT}\right) \quad (9)$$

where h is Planck's constant, N A Avogadro's number, R the universal gas constant, ΔH_a^* the enthalpy of the activation and ΔS_a^* is the entropy of activation.

Fig. 9 showed the plot of $\ln(1/R_tT)$ against 1/T. Straight lines were obtained with a slope of (ΔH_a^* /R) and an intercept of (ln(R/N A h) + (ΔS_a^* /R)) from which the values of ΔH_a^* and ΔS_a^* were calculated and listed in Table 4.

From Table 5, it seemed that Ea and ΔH_a^* varied in the same fashion. The values of Ea were higher for the inhibited solutions than that for the uninhibited solutions. According to Eq. (8), both Ea and A might affect the steel corrosion rate at a certain temperature. The influence of Ea on the steel corrosion was bigger than that of A on the steel corrosion. However, if the variance of A was drastically bigger than that of E_a, in this case the reduction of A (Table 4) was a decisive factor affecting the corrosion rate of C38 steel in 1 M HCl.

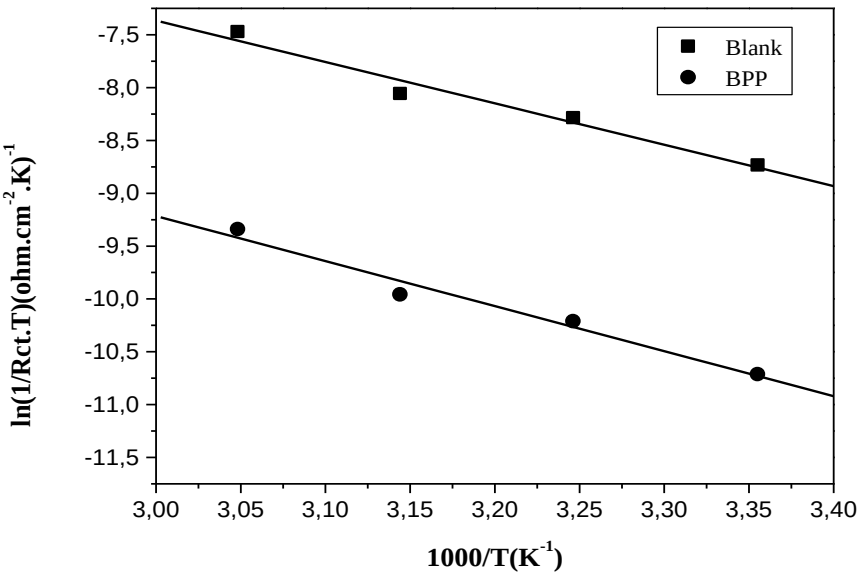

Figure 9. Arrhenius plots of steel in 1 M HCl with and without 10^{-3} M of **BPP**

The positive signs of ΔH_a^* reflected the endothermic nature of the C38 steel dissolution process. The value of ΔS_a^* is lower for inhibited solution than that for the uninhibited solution. This suggested that a decrease in randomness occurred on going from reactants to the activated complex. This might be the results of the adsorption of organic inhibitor molecules from the acidic solution could be regarded as a quasi-substitution process between the organic compound in the aqueous phase

and water molecules at electrode surface. Otherwise was noticed by Tao et al. in the study of inhibition mild steel by oxo-triazole derivatives where they attributed the phenomenon to the increase in the entropy of activation to the increasing in solvent entropy [42].

Moreover one remark that the ΔH_a^* values obtained from the slopes of plots log ($1/R_t.T$) versus f(1/T) and those determined from Eq. (10) are in good agreement.

$$\Delta H_a^* = E_a - RT \qquad (10)$$

Table 5. The value of activation parameters E_a, A, ΔH_a,ΔS_a and $\Delta \mathbf{G_{ads}}$ for steel in 1M HCl in the absence and presence of 10^{-3} M of **BPP.**

	E_a (kJ/mol)	Pre-exponential factor A ($\Omega.cm^2$)	ΔH_a (kJ/mol)	ΔS_a (J/mol)	ΔH_a (kJ/mol), calculated from Eq.10
Blank	35.13	6.5×10^4	32.54	-161.04	32.65
BPP	38.01	3.0×10^4	35.41	-167.79	35.53

4. CONCLUSIONS

The studied 3-bromo-2-phenylimidazol[1,2- α] pyridine (**BPP**) shows excellent inhibition properties for the corrosion of C38 steel in 1 M HCl at 298 K, and the inhibition efficiency increases with increasing of the **BPP** concentration. The inhibitor efficiencies determined

by weight loss, Tafel polarisation and EIS methods are in reasonable agreement. Based on the polarisation results, the investigated **BPP** can be classified as mixed inhibitor. The EIS spec-

tra are described well by a relatively simple structural model having only one time constant. The calculated structural parameters show increase of the obtained R_t values and decrease of the capacitance, C_{dl} , with **BPP** concentration increase. It is suggested to attribute this to the increase of the thickness of the adsorption layer at steel surface. The adsorption model obeys to the Langmuir adsorption isotherm and the negative value of the $\Delta G°_{ads}$ indicates that the adsorption of the **BPP** molecules is a spontaneous process. The high negative value of $\Delta G°_{ads}$ suggests that the inhibitive effect of **BPP** is due to the formation of a chemisorbed film on the metallic surface. The thermodynamic results confirm the chemisorptive nature of the BPP adsorption on the C38 steel.

ACKNOWLEDGEMENTS

Prof S. S. Deyab, Prof B. Hammouti and Prof R. Salghi extend their appreciation to the Deanship of Scientific Research at King Saud University for funding the work through the research group project No. RGP-VPP-089.

References

1. S Bilgiç, H Yılmaz, *Mater. Chem. Phys.***,** 79 (2007) 5.
2. U. J. Ekpe, P. C. Okafor, E. E. Ebenso, O. E. Offiong, B. I. Ita, *Bull. Electrochem.*, 17 (2001) 135.

3. S. A. Odoemelam, N. O. Eddy, *J. Surf. Sci. Technol.*, 24 (2008) 65.
4. S. Ramesh, S. Rajeswari, S. Maruthamuthu, *Mater. Lett*. 57 (2003) 4547.
5. M. Mihit, R. Salghi, S. El Issami, L. Bazzi B. Hammouti, E. Ait Addi, S. Kertit, *Pigm. Res. Tech.*, 35 (2006) 151.
6. A. Dafali, B. Hammouti, R. Mokhlisse, S. Kertit, *Corros. Sci.*, 45 (2003) 1619.
7. S. Kertit, R. Salghi, L. Bazzi, B. Hammouti, A. Bouchtart, *Ann. Chim. Sci. Mat.*, 25 (2000) 187.
8. H. Zarrok, H. Oudda, A. Zarrouk, R. Salghi, B. Hammouti, M. Bouachrine, *Der Pharm. Chem*. 3 (2011) 576.
9. M. Mihit, K. Laarej, H. Abou El Makarim, L. Bazzi, R. Salghi, B. Hammouti, *Arab. J. Chem*. 3 (2010) 55.
10. H. Zarrok, A. Zarrouk, B. Hammouti, R. Salghi, C. Jama, F. Bentiss, *Corros. Sci*. 64 (2012) 243.
11. K. Barouni, L. Bazzi, R. Salghi M. Mihit, B. Hammouti, A. Albourine, S. El Issami, *Mater. Lett*. 62(2008) 3325.
12. S. El Issami, L. Bazzi, M. Mihit, B. Hammouti, S. Kertit, E. Ait Addi, R. Salghi, *Pig. Res. Tech*. 36 (2007) 161.
13. M. Mihit, S. El Issami, M. Bouklah, L. Bazzi, B. Hammouti, E. Ait Addi, R. Salghi, S. Kertit, *Appl. Surf. Sci*. 252(2006) 2389.
14. S. El Issami, L. Bazzi , M. Mihit, M. Hilali, R. Salghi, El. Ait Addi, *J. Phys. IV*.123 (2005) 307.
15. S. El Issami, L. Bazzi, M. Hilali, R. Salghi and S. Kertit, *Ann. Chim. Sci. Mat*. 27 (2002) 63.
16. R. Salghi, L. Bazzi, B. Hammouti, S. Kertit, *Bull. Electrochem*. 16 (2000) 272.
17. L. Larabi, Y. Harek, O. Benali, S. Ghalem, *Prog. Org. Coat.*, 54 (2005) 256.
18. E.E. Oguzie, Y. Li, F.H. Wang, *J. Colloid interface Sci.*, 310 (2007) 90.
19. L. Larabi, O. Benali, Y. Harek, *Port. Electrochim. Acta*, 24 (2006) 337.
20. O. Benali, L. Larabi, B. Tabti , Y. Harek, *Anti-Corros. Met. Mat.*, 52 (2005) 280.
21. L. Larabi, O. Benali, S. M. Mekelleche, Y. Harek, *Appl. Surf. Sci.*,253 (2006) 1371.
22. O. Benali, L. Larabi, M. Traisnel, L. Gengenbre, Y. Harek, *Appl. Surf. Sci.*, 253(2007) 6130.
23. B. Hammouti, R. Salghi, S. Kertit, *J. Electrochem. Soc. India*. 47 (1998) 31.
24. H. Zarrok, A. Zarrouk, R. Salghi, Y. Ramli, B. Hammouti, M. Assouag, E. M. Essassi, H. Oudda and M. Taleb, *J. Chem. Pharm. Res*. 4(12) (2012) 5048.
25. Zarrouk, B. Hammouti, H. Zarrok, R. Salghi, M. Bouachrine, F. Bentiss, S. S. Al-Deyab, *Res Chem Intermed*. 38 (2012) 2327
26. H. Bendaha, A. Zarrouk, A. Aouniti, B. Hammouti, S. El Kadiri, R. Salghi, R. Touzani, *Phys. Chem. News*. 64 (2012) 95
27. F. Bentiss, M. Lebrini, M. Lagrenée, M. Traisnel, A. Elfarouk, H. Vezin, *Electrochimica Acta.*, 52 (2007) 6865.
28. O. Benali, M. Ouazene, *Arab. J. Chem.*, 4 (2011) 443.
29. H. B. Ouici, O. Benali, Y. Harek, L. Larabi, B. Hammouti, A. Guendouzi, *Res. Chem. Intermed.*, doi 10.1007/s11164-012-0797-1.
30. F. Bentiss, B. Mernari, M. Traisnel, H. Vezin, M. Lagrenée., *Corros. Sci.*, 53 (2011) 487.
31. F. Bentiss, M. Traisnel, L. Gengembre, M. Lagrenée, *Appl. Surf. Sci.*, 161 (2000)194.
32. T. Tsuru, S. Haruyama, B. Gijutsu, *J. Jpn. Soc. Corros. Eng.*, 27 (1978) 573.
33. A. K. Mohamed, T. H. Raha, N. N. H. Moussa, *Bull Soc. Chim Fr* 127 (1990) 375.
34. H. F. Finley, N. Hackerman, *J. Electrochem. Soc.*, 107 (1960) 259.
35. N. Hackerman, E. S. Snavely, J. Payne, *J. Electrochem. Soc.*, 113 (1966) 677.
36. H. Ashassi-Sorkhabi, S. A. Nabavi-Amri, *Acta. Chim. Slov.*, 47 (2000) 507.
37. I. B. Obot, N. O. Obi-Egbedi, *Corros. Sci*, 52 (2010) 198.
38. O. Benali, L. Larabi, S. M. Mekelleche, Y. Harek, *J. Mater. Sci.*, 41(2006) 7064.
39. J. D. Talati, D. K. Gandhi, *Corros. Sci.*, 23 (1983) 1315.
40. G. K. Gomma, M. H. Wahadan, *Indian J. Chem. Technol*., 2 (1995) 107.

41. Z. Szklarska-Smialowska, J. Mankowski, *Corros. Sci.*, 18 (1978) 953.
42. S. Zhang, Z. Tao, W. Li, B. Hou, *Appl. Surf. Sci.*, 255 (2009) 6757.